Supplementary Information for

# The relation between microstructure and photocatalytic behavior in lanthanum-modified 2D $TiO_2$ nanosheets upon annealing of a freeze-cast precursor

Snejana Bakardjieva[a*], Jakub Mares[a], Radek Fajgar[b], Victor Y. Zenou[c], Michaela Maleckova[d], Efthalia Chatzisymeon[e], Hana Bibova[f] and Jaromir Jirkovsky[f]

[a.] *Institute of Inorganic Chemistry of the Czech Academy of Sciences, 250 68 Husinec-Řež, Czech Republic. Email: snejana@iic.cas.cz*
[b.] *Institute of Chemical Process and Fundamentals of the Czech Academy of Sciences, Rozvojova 2/135, 165 02 Prague, Czech Republic*
[c.] *Nuclear Research Center-Negev, Department of Material Engineering, 841 90 Beer Sheva, Israel*
[d.] *Charles University, Faculty of Science, Hlavova 2030/8, 128 42, Prague, Czech Republic*
[e.] *School of Engineering, Institute for Infrastructure and Environment, The University of Edinburgh, Edinburgh, EH9 3JL, United Kingdom*
[f.] *J. Heyrovsky Institute of Physical Chemistry of the Czech Academy of Sciences, Dolejskova 2155/3, 182 23 Prague, Czech Republic*

*To whom correspondence should be addressed. e-mail: snejana@iic.cas.cz
/Snejana Bakardjieva/

## 1. STEM/EDS and elemental mapping

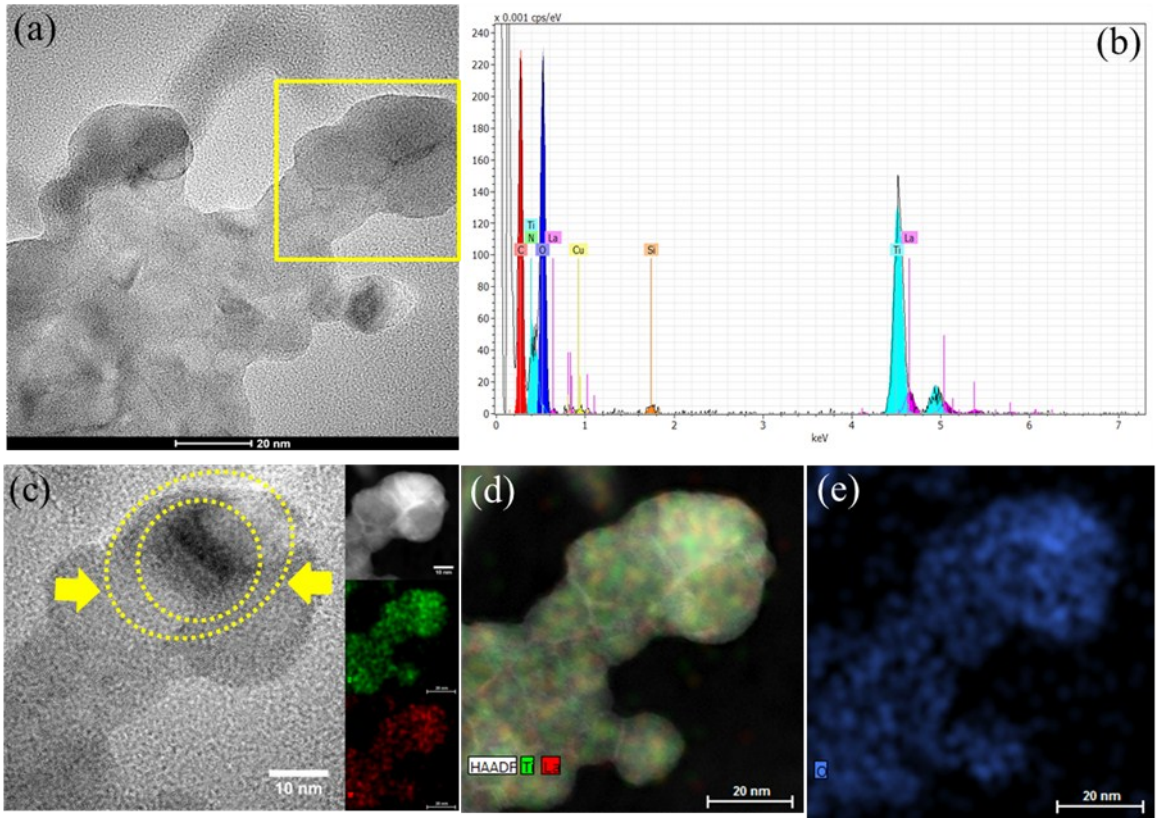


Fig.S1 STEM/EDS study of Ti_La_LYO (a) Low MAG STEM image, (b) EDS spectrum of yellow boxed area (c) High resolution STEM image with distribution of Ti and La (right columns), (d) the overlays of both Ti and La elements and (e) distribution of O element.

Figure S1/a presented low magnification TEM image of freeze-cast precursor Ti_La_LYO. The EDS spectrum (Fig.S1/b) of yellow boxed area showing significant Ti, La and O peaks (Cu and C peaks come from TEM grid, Si and N are negligible instrumental artefacts). High-resolution STEM image (Fig.S1/c) of the same boxed region as in Fig.S1/a, showing localities where elemental mapping was obtained. Right columns in Fig.S1/c presented the distribution of Ti and La elements. We observed from the two-colour overlay HAADF map in Fig.S1/d that Ti and La formed bi-nuclear cores (clusters) by approach each other. The high-resolution STEM image in Fig.S1/c shown an individual core brought into contact with a continuous ~ 5–10 nm thick amorphous shell (marked with yellow arrows). We have been found in our previous research (E. Plizingrova et al., 2015; J. Subrt et al., 2014) that freeze casting process of PPTA precursor, which is the the final yellow transparent solution with pH ~ 3, dripped into $LN_2$ and transferred into the lyophilizator (as shown in Scheme 1), resulted in condensation reaction of hydroxide and peroxo groups. The hydroperoxide groups can be formed simply on the surfaces of $TiO_2$ according to the reactions:

$$=Ti=O + H_2O_2 \rightarrow =Ti(OH)(OOH) \quad (1)$$

$$\equiv Ti\text{-}OH + H_2O_2 \rightarrow \equiv Ti\text{-}OOH + H_2O \quad (2)$$

yielded hydrolyzed $Ti^{4+}$ species (F.A. Cotton and G. Wilkinson, 1988; D. Klissurski et al., 1990). The elemental mapping in Fig S1/e revealed a uniform distribution of the high content of O element and supporting findings from equations (1) and (2). Our STEM/EDS examinations deduced that the surface of bi-nuclear Ti-La core is modified by the presence of surface hydroxide and peroxo groups. Therefore, we can conclude that as-observed unique amorphous shell is consisting of a great quantity of (-OH) and (-OOH) groups.

Formation of the amorphous shell could be regarded as the initial step of amorphous-to-crystalline $TiO_2$ transformation in an aqueous media. Infrared spectra (see Fig. 7 in manuscript) showed broad bands cantered at 3229 $cm^{-1}$ and 3417 $cm^{-1}$ assigned to the stretching vibration of O-H groups and sharp peak corresponding to water at 1625 $cm^{-1}$. The bands located at 3229 $cm^{-1}$ and 1625 $cm^{-1}$ decrease when the annealing temperature increases due to efficient desorption of surface water. Additionally, bands at 692 $cm^{-1}$ and 903 $cm^{-1}$ attributed to the vibration modes of peroxo -O-O-(H) groups were detected. Both peaks disappeared after annealing upon 500 °C due to the decomposition of -O-O-(H) groups. XPS measurements of the precursor Ti_La_LYO revealed that hydroxide ions are presented also. Our observations are in agreement with results previously published for nano-sized anatase crystallized from lyophilized PPTA (H. Ichinose et al., 1996; J. Subrt et al., 2014) confirming that the presence of water in the crystallization reaction catalyzes the rearrangement of the $[TiO_6]$ octahedra in the amorphous titania by adsorption to the titania surface, and increases the rate of crystallization significantly (K. Yanagisawa et al., 1999).

References:

Guido Busca, Heterogeneous Catalytic Materials: Solod State Chemistry, Surface Chemistry and Catalytic Behaviour, 2014 Elsevier, ISBN 978-0-444-59524-9.

E. Plizingrova, L. Volfova, P. Svora, N. Labhsetwar, M. Klementova, L. Szatmary, J. Subrt, Highly photoactive anatase foams prepared by lyophilized aquous colloids of peroxo-polytitanic acid, Catal. Today 2015, 240, 107-113,

J. Subrt, P. Pulisova, J. Bohacek, E. Plizingrova, L. Volfova, J. Kupcik, Highly photoactive 2D titanium dioxide nanostructures prepared from lyophilized aquous colloids of peroxo-polytitanic acid, Mat. Res. Bull. 2014, 49, 405-412.

F.A. Cotton and G. Wilkinson, Advanced Inorganic Chemistry, John Willey & Sons, 5th Edition, 1988, ISBN 0-471-84997-9.

D. Klissurski, K. Hsdjiivanov, M. Kantchva and L. Gyurova, J. Chem. Soc. Faraday Trans., 86, 385-88 (1990).

H. Ichinose, M. Terasaki, H. Katsuki, Synthesis of Peroxo-Modified Anatase Sol from Peroxo Titanic Acid Solution, J. Ceram Soc. Japan, 104 (8) 715-718 (1996).

K. Yanagisawa, J. Ovestone, Crystallization of anatase from amorphous titania using the hydrothermal technique: Effect of starting material and temperature, J. Phys. Chem. B 1999, 103, 7781-7787.

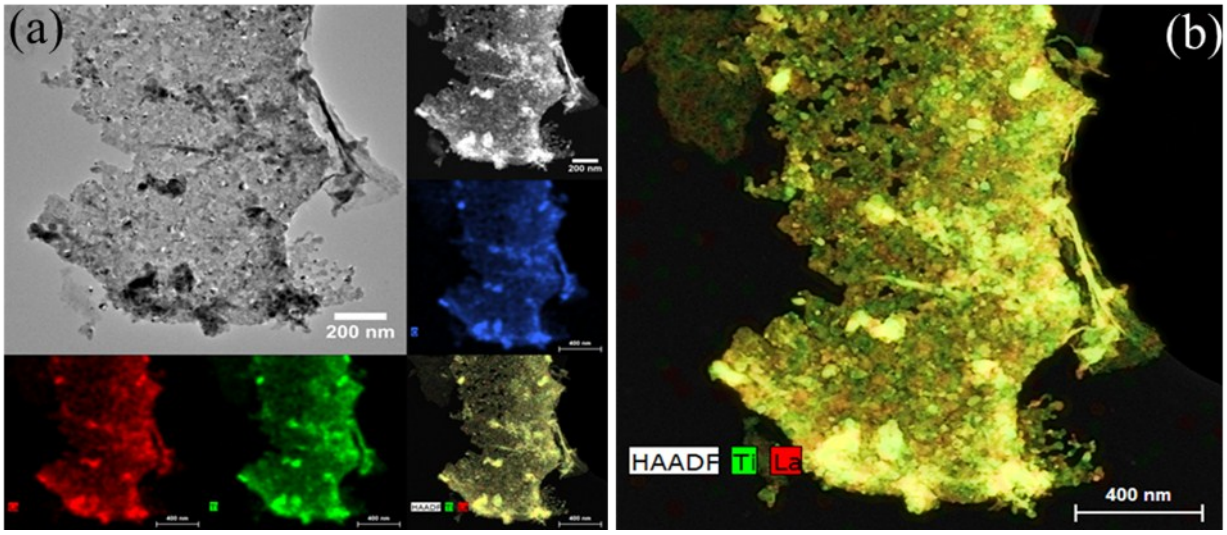


Fig.S2 STEM study of the precursor Ti_La_LYO (a) Low MAG STEM image and elemental mapping showing the distribution of Ti and La (the bottom row), the distribution of O element and overlays of Ti and La (the right column), (b) HAADF image showing overlays of two (Ti and La) elements.

## 2. Degradation of 4CP under UV irradiation.

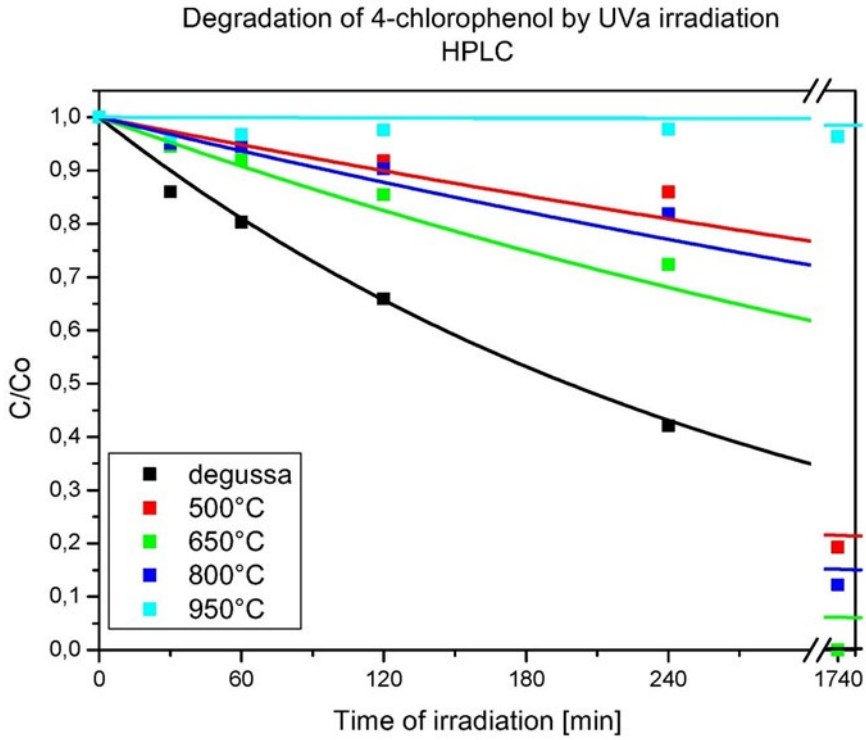


Fig.S3 The degradation curves of 4CP under UV irradiation light

## 3. UV-Vis reflectance spectra

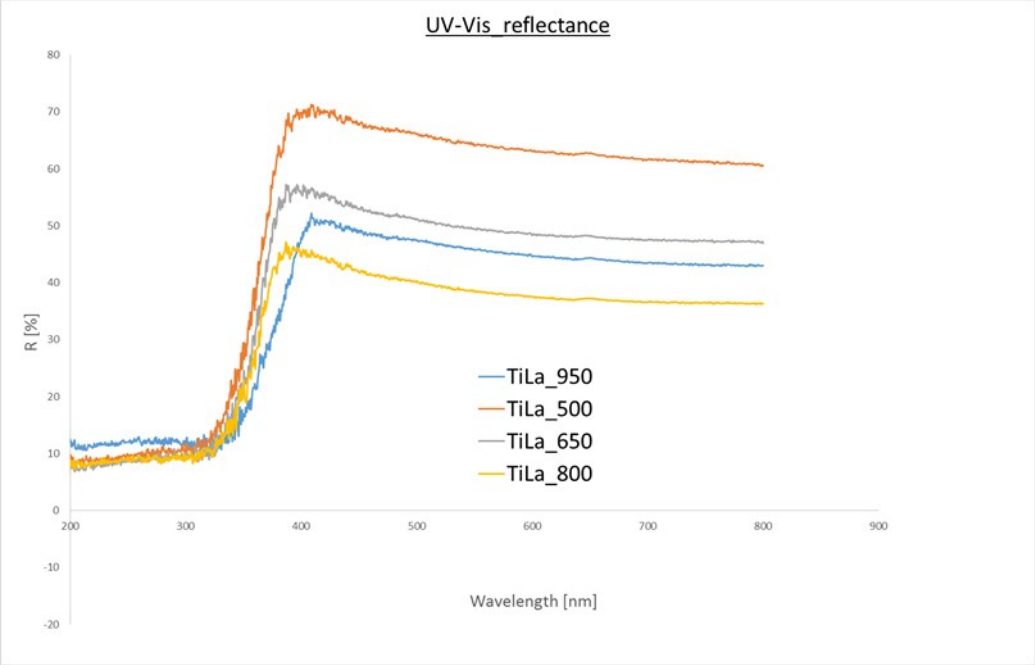


Fig. S4 UV-Vis reflectance spectra of the sample TiLa_500, TiLa_65 , TiLa_800 AND TiLa_950.

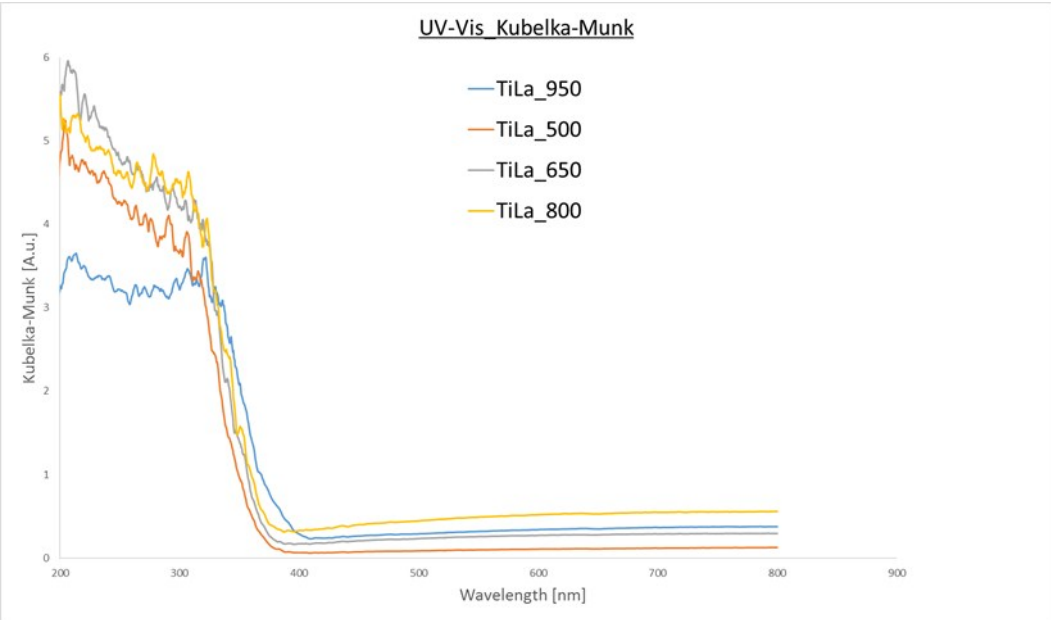


Fig. S5 Kubelka-Munk function of the sample TiLa_500, TiLa_65 , TiLa_800 AND TiLa_950 estimating the band gap energy ($E_{BG}$).

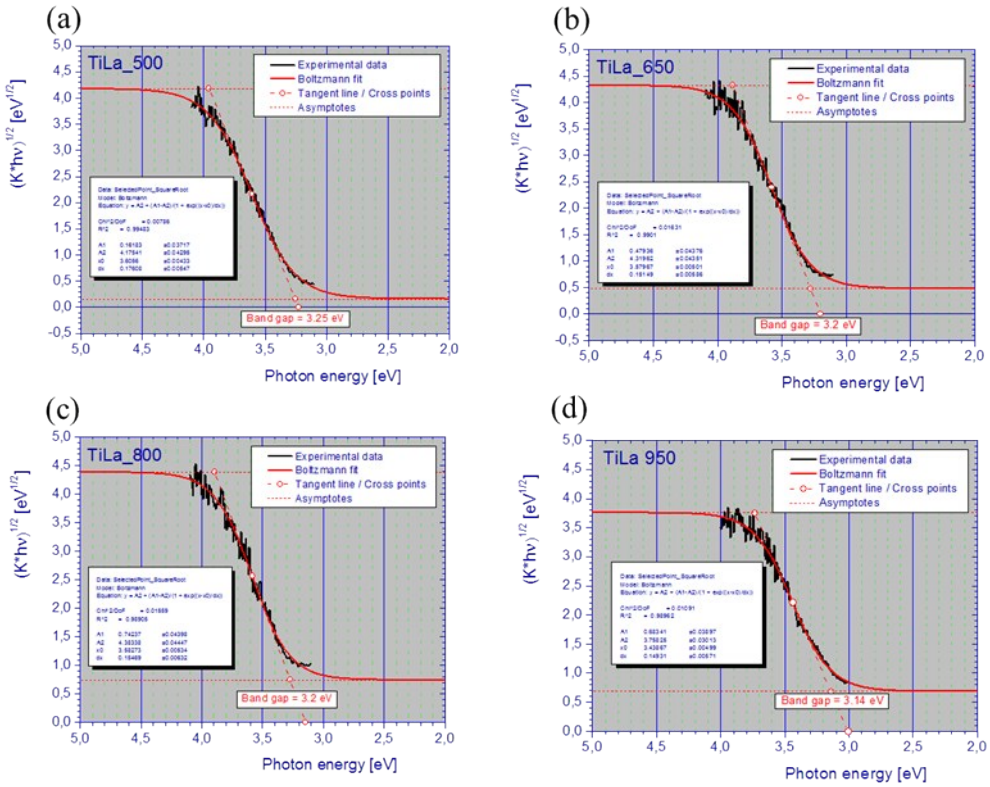


Fig. S6 The band gap energy ($E_{BG}$) of samples (a) TiLa_500, (b), TiLa_650 (c) TiLa_800 and (d) TiLa_950.

## 4. Degradation of 4CP by using Ti_La_950 under simulated solar light

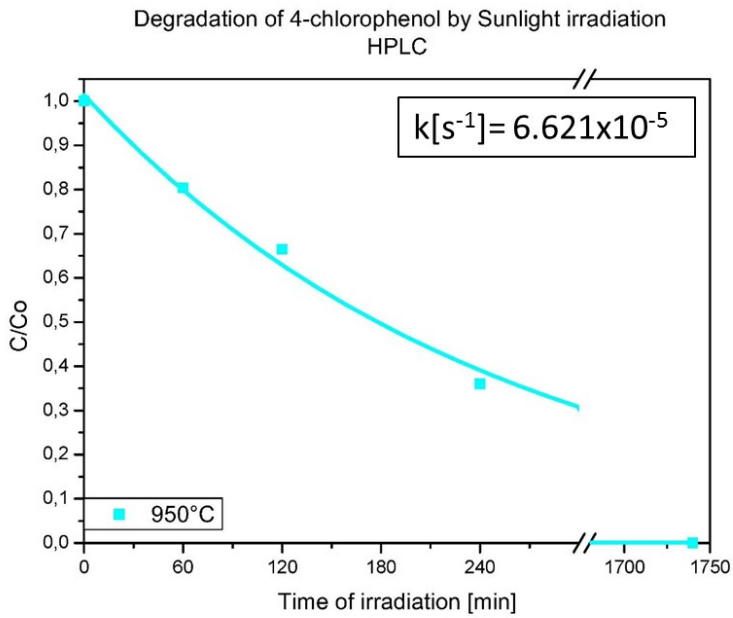


Fig.S7 Degradation of 4CP by Ti_La_950 under simulated solar light with calculated rate constant k [$s^{-1}$] (inset).